JOURNAL OF RAMAN SPECTROSCOPY
J. Raman Spectrosc. 2005; **36**: 400–408
Published online 1 April 2005 in Wiley InterScience (www.interscience.wiley.com). DOI: 10.1002/jrs.1305

JRS

A correlated method for quantifying mixed and dispersed carbon nanotubes: analysis of the Raman band intensities and evidence of wavenumber shift

Han Athalin* and Serge Lefrant
CNRS, Institut des Matériaux Jean Rouxel, Université de Nantes, 2, rue de la Houssinière, 44322 Nantes cedex 03, France

Received 28 July 2004; Accepted 29 November 2004

We present an experimental investigation of a correlated quantitative analytical method based on advanced Raman spectroscopy. This method was developed for the intensity weight distribution analysis of mixed and dispersed carbon nanotube (CNT) mixtures. For Raman spectroscopy, mixtures of single-walled CNTs (SWNTs) and multi-walled CNTs (MWNTs) were prepared and dispersed on a coverslip. Mixtures were made in the range from 1 to 100 mg (wt%) of SWNTs in 100 to 1 mg (wt%) of MWNTs. The ratios of the relative intensities of the Raman bands corresponding to pure SWNTs and pure MWNTs were used for the construction of calibration curves used for quantitative analysis. The relative intensity of the deconvoluted spectral bands shows a characteristic feature at 1350 and 1592 cm^{-1} which was found to be proportional to the relative amounts of SWNTs and MWNTs in the mixtures. A correlation between the atomic force microscopy images and the tangential mode Raman intensity ratio was used without the need for other analytical techniques. With this feature, it is possible to quantify the different components in the mixed, dispersed or unknown bulk of the CNTs investigated. Copyright © 2005 John Wiley & Sons, Ltd.

KEYWORDS: quantitative Raman spectroscopy; deconvolution; separation of mixtures; signal processing

INTRODUCTION

In this paper, we report a relationship between the Raman intensity ratio of selected peaks and the content of different mixtures of carbon nanotubes (CNTs) by the quantitative examination of these mixtures. To explain, briefly what dispersion means, raw nanotubes can create relatively stable suspensions (spaghetti-like strands) at high concentrations of solvents, otherwise nanotubes still exist as bundles of varying sizes, but separated individual nanotubes are not present. This can be defined as the macro-dispersion of nanotubes. In contrast, the individual dispersion can be defined.[1–3] A common feature of CNTs (single-component or mixed samples) when dispersed is often the arrangement in various directions, their morphology and their different densities on a coverslip surface or when embedded in polymers.[4–6] The disordered structure may be related to the sequence of deposition of the various types of the CNTs. Since the CNTs were discovered by Iijima,[7] Raman spectroscopy (RS) and other techniques have been employed for their analysis.[8–14] In a previous study, the potential of an ultra-narrow bandwidth laser as a light source for the diffraction-limited measurement of CNTs was demonstrated for selective nanovolume RS.[15] It is often very difficult, if not impossible, to identify all the components present in a mixture by using only one analytical technique. RS is convenient for both the qualitative and quantitative analysis of multi-component mixtures without degradation of the samples.[16] RS has the advantage of using a selected monochromatic laser beam which may be focused precisely and selectively over any part of a solid sample, which may consist of different components. No sample pretreatment is needed and the local composition of the CNTs can be analyzed quantitatively so that the various components analyzed give Raman-active spectral bands. In this paper, we focus on the methodology of the quantitative analysis of mixed and dispersed CNTs used in our laboratory for analysis. RS is not very sensitive to the physical appearance of the sample, which means that different phases (solid, liquid, gas) of samples can be studied directly without preparation of the sample, but it is sensitive to the conditions at the molecular level.

*Correspondence to: Han Athalin, CNRS, Institut des Matériaux Jean Rouxel, Université de Nantes, 2 rue de la Houssinière, 44322 Nantes cedex 03, France. E-mail: han@cnrs-imn.fr
Contract/grant sponsor: Conseil Régional des Pays de la Loire.

ATTRIBUTION OF THE D AND G BANDS

There are two predominant features in the Raman spectra of CNTs, the radial breathing mode (RBM) and the tangential

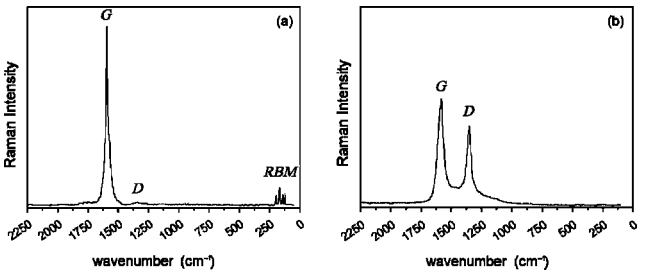

Figure 1. Typical Raman (normalized) spectra from CNTs. (a) SWNTs showing the RBM features, D- and G-band profiles in the TM mode. (b) D- and G-band profiles in the TM mode attributed to MWNTs. Pure SWNTs (physically different tubes) all exhibit an observable D-band signal with a weak intensity usually ~100 times smaller than the G-band. The Raman spectra of the pure forms are in good agreement with those published elsewhere.[12–26]

mode (TM). The Raman wavenumbers of the RBM (ω_{RBM}) bands appear between 120 and 250 cm^{-1} for single-walled CNTs (SWNTs) within 1 nm < d_n < 2 nm and correspond to the atomic vibration of the C atoms in the radial direction [Fig. 1(a)]. These features are very useful for characterizing nanotube diameters, d_n.[12,13,17] All carbon forms contribute to the Raman spectra in the range from ~1000 to ~1700 cm^{-1}. The observation of the characteristic multi-peak features around ~1580 cm^{-1} also provides a signature of CNTs, typically giving rise to a two-band feature with two peaks named the D-band (or disorder band) around ~1300 cm^{-1} and G-band around 1590 cm^{-1} in the first-order Raman spectra of CNTs [Fig. 1(a) and (b)].

The D-band in SWNTs is within the range ~1285–1300 cm^{-1} having a full width half maximum (FWHM) of ~10–30 cm^{-1}.[18] For crystalline graphite-like allotropes (i.e. fullerenes) and glassy carbon (pure carbon produced by the thermal decomposition of polymer), the D-band is found at ~1305–1330 cm^{-1} and the FWHM is ~30–60 cm^{-1}.[19] Multi-walled CNTs (MWNTs) exhibit D-bands with parameters close to those of the crystalline graphite-like allotropes. Second, the peak denoted the G-band is around ~1580 cm^{-1}, having an FWHM of ~5–30 cm^{-1}.[20,21] Generally, the doublet that appears around ~1553 and ~1589 cm^{-1} can be attributed to a combination of the A_{1g}, E_{1g} and E_{2g} vibrational modes, the wavenumbers of which are known to be weakly dependent on the nanotube diameter. The G-band for MWNTs is a single peak at 1582 cm^{-1} and the FWHM is $\gtrsim$70 cm^{-1}. In many cases, the G-band of MWNTs disappears with mixed samples,[22] which is why in our study we used the D-band at 1350 cm^{-1} with a laser wavelength of 532 nm for the analytical observation. The D-band usually creates ambiguities as to whether it should be assigned to non-SWNT samples or to defects on SWNTs. Even though calculations showed that SWNTs also have a weak contribution in this region, the D-band has been used for the estimation of sample purity.[23,24]

The two most intense G peaks of SWNTs are labeled G^+ at 1592 cm^{-1} assigned to semiconducting and 1587 cm^{-1} assigned to metallic, for atomic displacements along the tube axis. The G^- peak at 1570 cm^{-1} is assigned to semiconducting and at 1550 cm^{-1} assigned to metallic, for modes with atomic displacement along the circumferential direction. The linewidths G^+ and G^- for the G peaks from semiconducting isolated SWNTs are usually ~5–15 cm^{-1}. For semiconducting SWNTs in bundles, the linewidths are related to the diameter distribution. Otherwise, in metallic SWNTs, the linewidth is minor for G^+, whereas for G^- a significant linewidth occurs, and it is found that the linewidth for the Breit–Wigner–Fano (BWF) lineshape (broad and asymmetric peak) is strongly dependent on the tube diameter. The origin of the BWF profile is the quantum interference between the zone-center optical phonon and continuum electronic transitions around the same energy which can occur in the Raman signal of covalent semiconductors. This requires a continuum of electronic transitions, i.e. metallic SWNTs.[23] The asymmetric BWF lineshape is given by

$$I(\omega) = I_\Phi \frac{[1 + (\omega - \omega_{BWF})/q\Gamma]^2}{1 + [(\omega - \omega_{BWF})/\Gamma]^2} \quad (1)$$

where $1/q$ is a measure of the interaction of the phonon with a continuum of states, ω_{WBF} is the BWF frequency (ω) at maximum Raman intensity I_Φ and Γ is the broadening parameter. In order to analyze the Raman spectra quantitatively, they were fitted with Eqn (1) and a linear background using a least-squares fitting by a homemade subroutine in MathLab. For isolated tubes with d_n > 2 nm, G^- is similar to semiconducting SWNTs, and the band is fitted using a Lorentzian lineshape. Values of FWHM $G^- \gtrsim 70$ cm^{-1} have been observed for isolated metallic SWNTs. Therefore, this broadening is related to the presence of free electrons in nanotubes with metallic character.[23,25] Selective RS can also be used to distinguish between metallic and semiconducting SWNTs by their different G band lineshapes. The lineshape of this band depends on the excitation laser.[13] Spectra in this wavenumber range can be used for the characterization of nanotubes and their degree of disorder and/or entanglement can be extracted.

Otherwise, the position with relative intensity of the Raman peaks varies with carbon allotropes.[26] The intensity ratio of the 1350 and 1592 cm^{-1} bands has been used to quantify mixed and dispersed nanotubes. The FWHM ratio between the D- and G-bands is assigned to I_Φ (Φ_D/Φ_G) and the relative intensity between the D- and G-bands is assigned to Φ_I (I_D/I_G)[27] derived by the authors from the equation $L_a = 43.5/R_I$, which has often been used to validate the crystallinity from x-ray diffraction,[28,29] without any other consideration. Generally, the correlation of quantitation was not clarified but the authors concluded that 'by careful examination of the spectra, ... and further

JRS

investigation is needed'. Here, we extended the analytical methods used in RS experiments to allow reproducible, full quantitative/qualitative Raman spectra to be produced.

EXPERIMENTAL

Spatial resolution and instrument

To obtain reliable quantitative values from a three-dimensional (3D) microstructure, it is necessary to know the sample volume V from which the signal I_Φ is collected. The resolving power of the microscopes used by the RS systems based on classical focusing optics is restricted to certain limits. Two beams with wavelengths λ and $\lambda + \delta\lambda$ are resolved if the maximum of the diffraction pattern for one beam coincides with the minimum of the diffraction pattern for the other beam. This is known as the diffraction limit: this distance represents the diffraction-limited (DL) resolution of the microscope. For the lateral dimension, the Rayleigh length is given by $\delta r = (0.61\lambda/N.A.)$, where λ is the wavelength and $N.A.$ is the numerical aperture, defined by $N.A. = \eta \sin\alpha$, where η is the refractive index and α is the half-aperture of the imaging optics. According to a similar criterion, the axial resolution is given by $\delta z = 2\eta\lambda/(N.A.)^2$. The values δr and δz allow one to define a DL volume which corresponds to the 3D resolution of the confocal microscope (CM). By using a single-line Nd:YAG 532 nm laser (GCL-S from L.2000) with a very narrow bandwidth (up to 0.001 nm), we could spectrally resolve each selected sampling area within the CM detection volume. In this work, the laser wavelength 532 nm was used for all measurements; in addition, a 633 nm single-line source (iPac from Toptica Photonics) was also used for verification. In the CM-powered RS system of our setup, the spatial resolution achieved is about $\sim\lambda$ with a high-quality TEM_{00} laser to perform imaging without geometric aberration with the dry objective. In this setup, a high-resolution computer-controlled piezo-motor (PIFOC P-720 from P.I.) is attached to the focus control and the focal plane of the objective is systematically moved in discrete steps through the sample. A 60× (*N.A.* 1.2) dry objective (UPLAPO 60× from Olympus) was used both to focus the laser and to collect the scattered radiation in an epi-illumination configuration.

To collect essential Raman spectra, the scattered light after the CM is focused into the entrance slit of a holographic axial transmissive imaging spectrograph (Holospec 5000R from Kaiser), which provides an extremely high throughput.[30] In addition, the laser residence time is minimized, which prevents the sample from being burnt by overexposure to the laser. The aperture ratio of $f/1.8$ provides a 5–20 times greater collection angle than spectrographs operating at $f/8$. This RS system was chosen for its high sensitivity and stability. The focus lens and the spectrometer entrance slit are chosen so that the focal point is at the entrance slit of the spectrometer and the solid angle of the focused beam is f-matched to the spectrometer system. In this way, maximum collection efficiency and high-resolution spectroscopic information with an accuracy of $\sim$1 cm^{-1} for the Raman peaks are simultaneously obtained. A SuperNotch Plus filter is positioned before the entrance slit, which attenuates the Rayleigh scatter by over six orders of magnitude and allows the collection of data at Stokes shifts as low as 50 cm^{-1} and the simultaneous collection of both Stokes and anti-Stokes data. The Raman spectra were collected using an advanced thermoelectric (Peltier) cooled back-thinned intensified charge coupled device (ICCD) with a photon counting capability (DH 734 from Andor) mounted on the exit port of the spectrometer.

Raman intensity calibration

Raman spectral intensities are directly correlated with concentration.[16] This assumes that no other changes in the system and samples occur. For a quantitative analytical experiment, the Raman spectrum L_Φ of a sample, measured on a spectrometer, depends on several parameters,[31] which can be divided into three classes:[32] (i) laser excitation energy, (ii) sample volume and (iii) the totality of the light collection. Therefore, the optical setup for sampling and collection is optimized, then the inherent stability of the Raman signal intensity needs to be known for the experiments. In most published work on RS, the intensity calibration is concerned with the calibrating detector spectral response, rather than the detecting signal intensity across the spectrum.[33–35] Owing to the variety of RS setups, an external standard needs to be used to characterize the likely error in a quantitative experiment and calibrate the spectrometer. This is to allow spectra from different spectrometers to be compared, and then compared with published results. This aspect is important for the present work. The spectrum measured can be written as the result of the convolution product of the Raman signal of the sample by the apparatus function of the spectrometer, the whole then being multiplied by the detector response and expressed as

$$L_\Phi = R_d(\pi K I_\Phi) \tag{2}$$

where I_Φ is the Raman intensity emitted by the sample, π the apparatus function of the spectrometer, R_d the detector response and K is the convolution product.

In this setup, the detector response was checked using an Hg–Ar light source (from Oriel) which showed variations, because the quantum efficiency of the ICCD is never totally uniform over the entire back-thinned chip. Pixel-to-pixel variations in quantum efficiency are typically 0.05%. Hence any intensity fluctuations are likely to be due to the laser. Therefore, a sample of diamond mounted on a coverslip was used as the external standard with a strong and single peak at 1332 cm^{-1}. The calibration procedure used here is to sum intensity kilocounts per second [I(kcts s^{-1})] scans, which are collected several times and then averaged. This gives an average over the time period where intensity fluctuations occur.

In order to use RS to monitor these variations, the relative cross-sections for Raman scattering from diamond and CNTs were determined. The integrated intensities of the Raman spectra, recorded at an excitation wavelength of 532 nm, were then used to determine the weight% (wt%) of CNTs in order to give an indication of the spectral efficiency factor (SEF). This SEF can be compared and used as an indication of the optimum experimental parameters. Similar data using a 633 nm laser were also obtained. A curve-fitting sub-routine was developed with an analytical software (MathLab) for the Raman spectra in order to determine the ratio of the integrated intensity of wavenumber $\nu = 1332\ \mathrm{cm}^{-1}$ diamond band ($\nu_{\mathrm{reference}}$) with that of the total integrated intensity ($I^{\max}_{\mathrm{G-band}}$) of the CNT Raman spectrum. In the relative Raman cross-sections of CNT spectra we found that the diamond total integrated intensity with axes in the ⟨100⟩ direction differed by a factor of 233 for pure SWNTs and 195 for pure MWNTs during our experiments. Therefore, the diamond total integrated intensity is 233 times greater than CNTs globally. It is then possible to determine an SEF for CNTs. The SEF, E_Φ, for the Raman spectra excited by 532 nm laser radiation was calculated using the following equation:

$$E_\Phi = \frac{\nu_{\mathrm{reference}}}{\nu_{\mathrm{reference}} + (I^{\max}_{\mathrm{G-band}}/233)} \times 100 \qquad (3)$$

The correlation coefficient was 100, which means that the SEF is coherent. In our experiments, the Raman spectra of the pure forms are in good agreement with the equation used. The SEF was compared with the experimental parameters for each spectra. Using this procedure, a calibration should be valid over each sampling. The Raman intensity of this single peak was measured from the baseline. Therefore, baseline corrections were applied to all spectra to remove the small fluorescent/luminescent background. They were then optimized using Eqn (2) as the highest signal.

Mixing and dispersing process of CNTs

Highly purified CNTs (SWNTs part BU-203 and MWNTs part BU-201) were purchased from Bucky USA. In our investigations, the mixed and dispersed CNTs were used without further purification, as shown in Fig. 1. The average diameters of most of the SWNT and MWNTs were in the range 0.8–1.4 and 5–17 nm, respectively, according to RS and atomic force microscopy (AFM) investigations, as shown in Fig. 2.[36–38] The MWNTs and SWNTs were dispersed separately in toluene by high-energy sonication using an ultrasonic wand dismembrator. The high-energy sonication times ranged from 5 to 40 min. The SWNT and MWNT suspensions were subsequently mixed in a bath sonicator for 30 min. Different types of binary mixtures were prepared: mixtures were made containing 1, 5, 20, 40, 65 and 100% (percent of total weight in mg) of SWNTs in MWNTs (100, 65, 40, 20, 5 and 1%) (measured by Scientech SA-80 analytical balance). The mixture was then cast into a scientific grade coverslip and the toluene was allowed to evaporate completely. The purity and structure of the dispersed mixture of the CNTs were investigated using a Raman spectrometer with laser excitation wavelengths of 532 and 633 nm. Spectra were obtained of CNTs and of binary mixtures in each step.

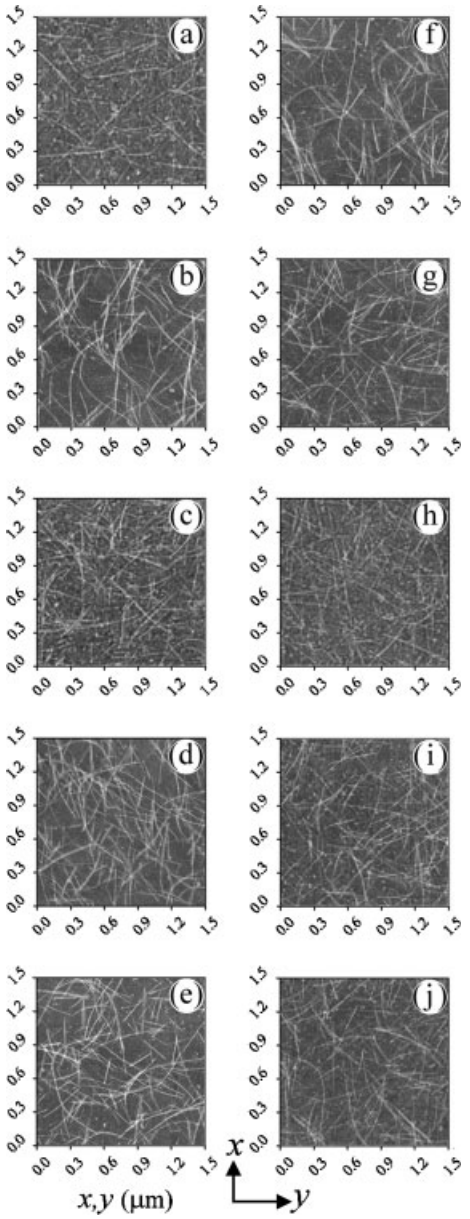

Figure 2. AFM (Dim 3100, Veeco) topographic images obtained during mixing to study the homogeneity of the CNT mixtures. (a)–(e) Mixtures consisting of 1, 5, 20, 40 and 65% (wt% in mg) of SWNTs in MWNTs (100% w/w) form, respectively; (f)–(j) mixtures consisting of 65, 40, 20, 5 and 1% (wt% in mg) of MWNTs in SWNTs (100%, w/w) form, respectively. In addition to CNTs, the topographic image shows in some cases a large number of small circular features with a height of ∼2–4 nm which are due to condensed water and removed by the laser excitation heating. Therefore, no Raman scattering signal is detected from humidity.

JRS

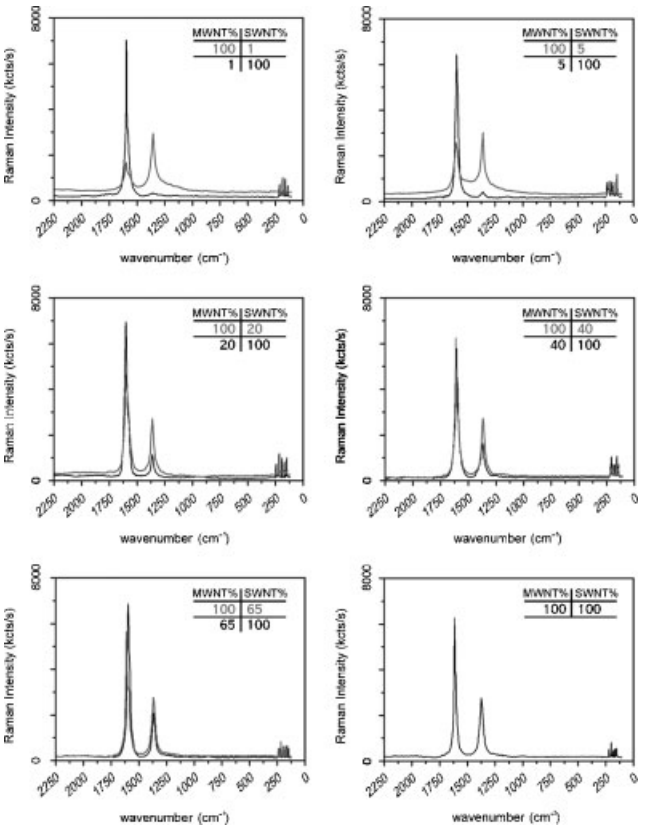

Figure 3. Evolution of the Raman spectra of the mixed samples. It is clear that with the increasing amount of SWNTs in the sample, the intensity of RBM and the G-band gradually increases, whereas that of the D-band decreases.

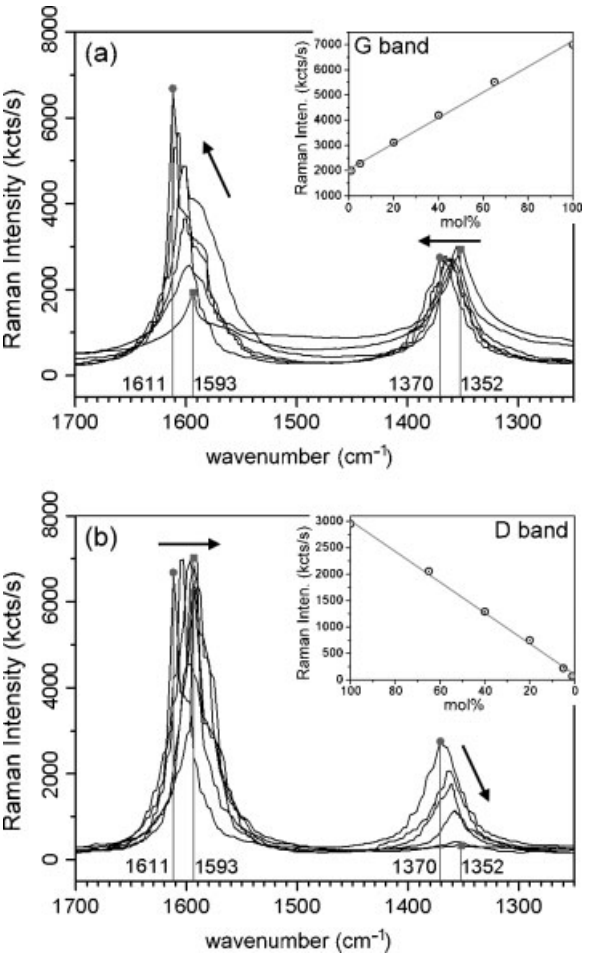

Figure 4. Linear regression TM spectra of CNTs (a) with mixtures consisting of 1, 5, 20, 40, 65 and 100% (wt% in mg) of SWNTs in MWNTs (100%, w/w) form. The inset shows the linear fitted data from Eqn (4); (b) with mixtures made linear consisting of 100, 65, 40, 20, 5 and 1% (wt% in mg) of MWNTs in SWNTs (100%, w/w) form. The insets are the linear fitted data from Eqn (4).

The mixtures were confirmed to be homogeneous by AFM, giving two-dimensional (2-D) images [Fig. 2(a)–(j)] and by obtaining a constant Raman spectrum at a variety of positions within them, but at a constant depth just on the samples (by a piezo-controlled objective). Figure 3 shows that the Raman spectra were measured from 80 to 2250 cm^{-1} under the same experimental conditions: laser power on the sample 200 μW, exposure time 2 s, one accumulation. Moreover, the position of the optical system (filter angles, slit, CM) was fixed for one selected excitation energy. For all the mixtures of CNTs, the sampling volume can be determinated from the DL volume of CM, as illustrated in section 'Spatial resolution and instrument'. Each Raman spectrum was collected three times: (i) accruable Raman signal, (ii) verification and (iii) confirmation; the selected area and the representative spectrum are a median of the measured spectra instead of their average. This procedure allows the elimination of dark signals and cosmic rays. The homogeneity of the mixed CNTs was verified by obtaining several Raman spectra from each mixture by focusing the laser beam on randomly selected parts of the dispersed sample. High correlations were observed with a linear regression fit on the spectrum and the concentration of analyte error A_e was calculated using the following equation:

$$A_e = C(\%)\sqrt{\left(\frac{e_b}{b}\right)^2 + \left(\frac{e_m}{m}\right)^2} \quad (4)$$

where $C(\%)$ is the weight concentration of analyte, b is the intercept, m is the slope, e_b is the standard error of y and e_m is the standard error of x coefficients. The results obtained are shown in the insets in Fig. 4.

METHODS OF ANALYSIS

Quantitative determination of scattered energy

In contrast to other analytical techniques, RS probes differences in the influence of the solid state on molecular spectroscopy. As a result, there is often a severe overlap of the majority of the spectral features for different forms

of the nanotubes, e.g. the G-band of MWNTs. The RS of the mixed CNT samples is related to the characteristics and the content of each CNTs component. Otherwise, the I_D/I_G value increases with increasing disorder and with decreasing crystallite size for each CNT component. However, RS of the I_D^{MWNTs}/I_G^{SWNTs} value, independent of the wavelength of the laser, is used to resolve quantitatively the relationship between the Raman scattering characteristics of the mixed samples. Sometimes, a complete resolution of the vibrational modes of a particular functional group suffices to differentiate the nature of the sample and allows direct quantification.

The overlap of spectral features results in a need for more approaches for quantification. Of the spectroscopic methods which have been shown to be useful for quantitative analysis, RS is perhaps the most responsive to quantification.[39] Since the nanotubes are dispersed in any medium like a metallized surface for surface-enhanced Raman scattering (SERS) spectroscopy, the latter is also applicable for the qualitative/quantitative analysis for nanotubes. The Kubelka–Munk equation is used to describe quantitatively the diffusely reflected radiation:[40]

$$F(R_\infty) = \frac{(1 - R_\infty)^2}{2R_\infty} + \frac{2.303ac}{\sigma_\Phi} \tag{5}$$

where $F(R_\infty)$ is the Kubelka–Munk function. The diffuse reflectance for infinitely thick samples (R_∞) is given by the reflectance of a sample of finite thickness (R_{sample}) divided by the non-absorbing reference ($R_{reference}$), a is the molar absorption coefficient, c is the molar concentration of the analyte and σ_Φ is the scattering coefficient. Scattering coefficients depend weakly on photon energy, but absorption cross-sections increase abruptly as electronic transitions become possible with increasing incident photon energy.

Clearly, for a linear relationship between intensity and concentration to exist, the scattering coefficient must be constant. At low analyte concentrations, the scattering coefficient will depend on the non-absorbing dispersant, whereas at higher concentrations, the linearity of RS analysis may be limited by the analyte. In developing a quantitative method based on vibrational spectroscopy, measures must be taken to ensure reproducibility. Unique spectral features must be identified and calibration studies must be performed on samples, described by Eqn (3), of known composition using peak areas determined by the integration required.

Raman response from mixed and dispersed CNTs

A single particle irradiated by a laser beam emits a radiant flux, Φ,[16] which can be expressed as

$$\Phi = \Phi_R + \Phi_E + \Phi_F + \Phi_T + \Phi_N \tag{6}$$

The Raman scattering, Φ_R, is always accompanied by elastic scattering, Φ_E, and thermal radiation, Φ_T. Further contributions can come from fluorescence, Φ_F, and non-linear emissions, Φ_N, such as stimulated Raman scattering or lasing. While the elastic scattering Φ_E occurs at a different wavelength than the Raman scattering and can therefore be filtered out with suitable devices, the other contributions usually cannot be separated from the Raman scattering and various smoothings with filtering algorithms have also been widely applied to improve the analytical signals.[15] The intensity of a Raman line depends on a number of factors, including the incident laser power, the frequency of the scattered radiation, the absorptivity of the materials involved in the scattering and the response of the detection system.

For the mixtures, complete deconvolution of the analyzed bands was achieved by employing a commercial spectroscopic package (OriginPro, Grams, PeakFit). Therefore, the area under the curve $I_{(\Phi)}$ of the separated bands was used for the quantitative determination of the two forms in mixtures. The measured $I_{(\Phi)}$, which is analogous to the Beer–Lambert law,[41] can be expressed as

$$I_{(\Phi)} = \varphi_0 k_v C V \sigma_A(\omega_0, \omega_s, T, C_i) \tag{7}$$

where φ_0 is the radiant flux density of the incident laser beam, v is the wavenumber in cm^{-1}, C is the concentration of the analyte, k_v is the ratio between the most intense peak and the others (or itself) of the Raman spectrum in the pure compound (or standard) and V the probed volume. The scattering cross-section, σ_A, depends on the frequency of the laser, ω_0, the frequency of the scattered radiation, ω_s, and the temperature, T, of the sample.[42] In general, the Raman scattering cross-section of a substance in a mixture of i substances is not independent of the composition of the mixture but depends on the concentration, C_i, of each substance and considering that the normalized intensity of a Raman peak can be expressed as

$$I_N^v = \frac{s}{k_v} C \tag{8}$$

where s is a proportionality coefficient. By considering the normalized intensity in Eqn (8), an expression for the Raman intensity of the single component is obtained when the Raman spectra in different concentrations can be written from the pure compound and can be expressed as

$$I_\Phi^v = \frac{I_x^{max}}{100} \frac{s}{k_v} C \tag{9}$$

where I_x^{max} is the intensity of the most intense peak in the Raman spectrum for a given pure compound. In the expressions, k_v is allowed to change the slope value for each peak and, with these new values, the predicted curves for the less intense peaks can be found. Meanwhile, the intensity is normalized, the value of s of the most intense peak may be given from the analysis of the Raman spectrum for the pure compound and two for the (same) pure compound

JRS

in the concentration range of interest. By superposition and Eqn (9), we can obtain an expression depending on the concentrations. For this, it is considered that each data point in the spectrum of the mixture presents an intensity given by the sum of the equivalent points in the compound spectra which have to be scaled according to their respective concentration C.

$I_{(\Phi)}$ depends on both numerous instrumental factors and the sample, which explains the difficulty in determining absolute intensities as we described. As the scattering intensity is proportional to the concentration of the scattering CNTs, it is possible to acquire quantitative information about a mixture. To determine how the individual components contribute to the Raman spectrum of a mixture, raw spectra of the nanotubes are required, as seen in Fig. 1. Any set of spectral data consists of a finite number of intensity values measured at discrete and equidistant wavenumbers. Each spectral data point contains a contribution from all components in a mixture. It is assumed that there is a linear relationship between Raman intensity and the molar density of a substance.

To solve for the individual contributions requires the application of multiple linear regressions or principal component analysis. Each data point in the spectrum of the mixture has an intensity given by the sum of the equivalent data points in the component spectra which have been scaled according to their respective concentrations. Rearranging Eqn (7), it can be seen that for a particular component x, the instrumental factors can be expressed in terms of measurable quantities:

$$k_x V = \frac{I_\Phi^x}{\varphi_0^x C_x^{\text{pure}}} \tag{10}$$

Therefore, it can be deduced for a mixture composed of the D-band represented by M for MWNTs and G-band represented by S for SWNTs that

$$I_\Phi^{\text{mix}} = I_M^{\text{mix}} + I_S^{\text{mix}}$$
$$I_\Phi^{\text{mix}} = \left[\frac{\varphi_0^{\text{mix}}}{\varphi_0^M}\right]\left[\frac{C_M^{\text{mix}}}{C_M^{\text{pure}}}\right]\varphi_0^{\text{pure}} + \left[\frac{\varphi_0^{\text{mix}}}{\varphi_0^S}\right]\left[\frac{C_S^{\text{mix}}}{C_S^{\text{pure}}}\right] I_S^{\text{pure}} \tag{11}$$

where C_M^{mix} and C_S^{mix} are the concentrations of components M and S in the mixture. Provided that the spectra of the pure components are recorded at the same laser power, the dependence of the spectral intensity in the mixture on the laser power is represented by a constant multiplicative factor. Furthermore, when the laser power is kept constant throughout ($\varphi_0^{\text{mix}} = \varphi_0^M = \varphi_0^S$), as is the case for the experiments reported here, the expression is reduced to

$$I_\Phi^{\text{mix}} = p_M I_M^{\text{pure}} + p_S I_S^{\text{pure}} \tag{12}$$

where p_M and p_S are the concentration proportions of M and S. These values represent the proportions of M and S in the mixture assuming that it is ideal. Therefore, as many studies show, pure SWNTs have very small I_D/I_G values, assumed to be 0.01,[43–45] as seen in Fig. 1(a) and if there are some impurities in the selected components it means that SWNTs or MWNTs can also be determined by Eqn (11). Given that Raman scattering depends on the number of molecules, then in a mixture with two components illuminated and viewed, the concentration proportion is the mole fraction.[46] Therefore,

$$p_M = \frac{n_M}{n_M + n_S} \tag{13}$$

and

$$p_S = \frac{n_S}{n_M + n_S} \tag{14}$$

where n_M and n_S are the number of moles of M and S, respectively, in mixed product $p_M + p_S = 1$. The present spectral observation on the samples provides a useful tool for the quantitative analysis of selected components in mixed and dispersed CNTs.

RESULTS AND DISCUSSION

For mixed and dispersed CNTs, the D- and G-bands were chosen for the analysis. In order to find the proper coefficients to be ascribed in Eqn (7), the analysis of the Raman intensities of the pure CNTs and mixture of CNTs at concentrations of 1, 5, 20, 40, 65 and 100% (percent of total weight) was carried out. The experimental data are presented in Fig. 3. It is clear that with increasing amount of SWNTs in MWNTs, the intensity of RBM and the G-band gradually increases, whereas that of the D-band decreases. It was found that the baseline is decreased by the increment of SWNTs in MWNTs. The D- and G-bands of the mixed samples all shift to higher wavenumber by 18 cm^{-1} with increasing amount of SWNTs (Fig. 4). Therefore, a detailed analysis of the G-band of MWNTs entirely overlaps by a combination of Raman modes when the content of SWNTs is ~2–3 wt%, as seen in Fig. 5. It is profile broad and asymmetric and it is well described by a BWF component. This result indicates that the Raman scattering characteristics of the mixed samples are related to the characteristics and the content of each carbon component.

The experimental data for the two TM bands of the MWNTs and SWNTs were used as examples; they were compared with the predicted data using the respective values, and good correspondence was found. Figure 6 shows that, in the analyzed range of SWNTs content, the calculated $I_D^{\text{MWNTs}}/I_G^{\text{SWNTs}}$ values of the samples are in agreement with the measured data. The Raman spectrum for each of the mixtures was predicted by Eqn (11) and the concentrations of the compounds were found for comparison with the experimental spectrum. In the results relating to the spectral regression of the CNTs in the mixture, we observe several important points:

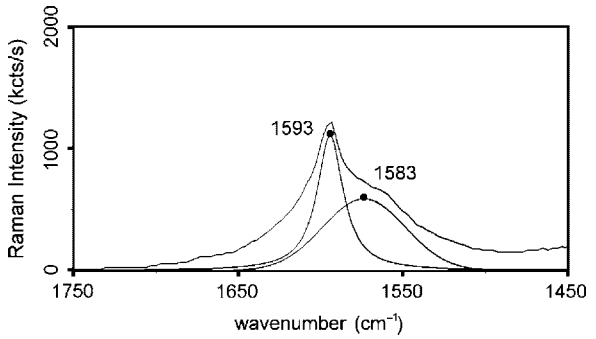

Figure 5. Deconvolution analysis of the intensity of the G-band in mixed samples (1% SWNTs in 100% MWNTs). The G-band of MWNTs (pure component G-band at 1580 cm^{-1}) weakens on adding an SWNT (pure component G-band at 1592 cm^{-1}). The G-band of MWNTs disappears when the content of SWNTs is ~2–3 wt% and it was deconvoluted into a double band by a Lorentzian and Gaussian component.

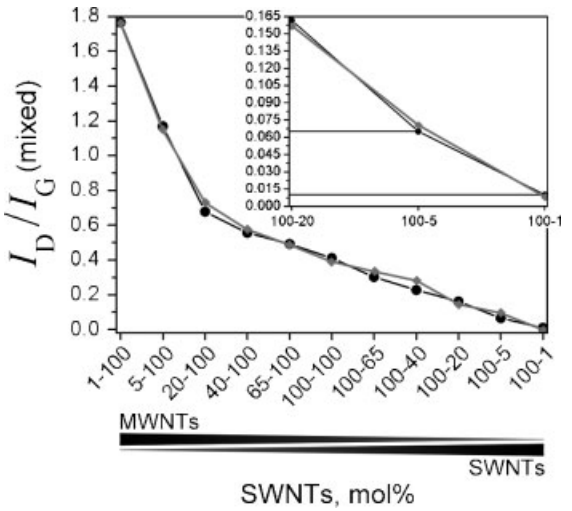

Figure 6. Measured (●) and calculated (♦) I_D^{MWNTs}/I_G^{SWNTs} values of the mixtures made linear in the range from 1 to 100% (wt% in mg) of SWNTs in 100 to 1% (wt% in mg) MWNTs form. The inset shows the detailed region.

1. It is possible with intensity-calibrated RS to distinguish clearly between the SWNTs (and also mostly semiconducting or metallic) and MWNTs in the mixed and dispersed bulk area. The clearest difference is seen for the D-bands for the MWNTs and G-bands for the SWNTs. These bands are in a region characteristic of conjugated Raman wavenumbers of CNTs. However, this suggests that a conjugated Raman wavenumber CNT in one sampling area gives generally clear spectra in routine CNT experiments. As a consequence, the interpretation of complex experimental Raman spectra in reliable and absolute terms is difficult without references. Nevertheless, it represents more or less some kind of random RS studies that do not allow a real selection of a desired nanovolume molecule. Therefore, it is also necessary to develop local probe techniques.[47]
2. The ratios of the relative intensities of the characteristic peaks of the two components present in a mixture of known composition (w/w), were found to depend linearly on the inverse of the SWNT concentration. The relationship can be expressed in a linear calibration curve.
3. In a mixture, where the identification of the most intense peaks is in some cases not possible owing to overlapping,[48] the relation $k_{(\nu)}$ allows us to consider any other peak of the Raman spectrum for quantitative analysis. In addition, we observed that the slope value for the most intense peak takes a value of almost one at high concentration (volume percentages).
4. The lower limit of concentration studied in the present work was 1% S in 100% M (w/w) and was confirmed in a deconvoluted G-band spectrum as seen in Fig. 5. This concentration was limited by the difficulty in mixing the two CNT forms.
5. An additional result of the present method is that it yields information on the degree of homogeneity in the distribution of SWNTs and MWNTs over the sample.
6. Finally, the correlation between the topographical image obtained from AFM and the TM parameters obtained from CM-powered RS analysis demonstrated that RS is a fast and better method than AFM image quantification, using relatively simple equipment, for obtaining and quantifying mixed and dispersed CNTs in matrices. This method also has the advantage of using large 3D sample volumes rather than the essentially 2D non-spectroscopic image used in the AFM surface topographical method. However, it needs a relatively long time (from many minutes to several hours).

Some points of caution have to be kept in mind with a method such as that described here. The absolute intensity of the Raman signal is dependent on the size of the particles. There has been confusion in the literature about the nature of the relationship, but a different study shows Raman intensity growing with decreasing particle size. Hence when methods such as the present approach are used on production batches, one must ensure that the variation in CNT size is limited, or at least that the variation in particle size is similar for the different components in the mixture. Another point of caution is the heating of the sample which can take place even with a 532 nm laser. Any heating effects were below the limit of detection. We would like to comment that for many practical applications of RS it is preferable to use an instrument where an acceptable signal intensity is obtained with a single accumulation with long integration times rather than multiple accumulation with short integration times.

The above mathematical expressions were applied to the analysis of mixtures of CNTs, for the quantitative analysis of concentration and also for the analysis of active compounds. Moreover, this method can be extended

to evaluate multiple mixtures. We would expect that the mathematical expressions could be applied to CNT mixtures and complemented for the quantitative analysis of such mixtures by intensity-calibrated RS, as we have demonstrated in the section 'Raman intensity calibration'.

CONCLUSIONS

An alternative mathematical model has been presented which was used to determine the concentration and quantification of CNTs in a given mixture. The work clearly demonstrates that RS can now be used to produce quantitative concentration spectra of very complex 3D structures on the nanometric length scale. The confirmation of the linearity of the Raman data and the good reproducibility and detection limit and high correlation coefficients for the regression equations render the suggested analytical Raman method suitable for the rapid identification and quantitative determination of SWNTs and MWNTs in a dispersed mixture. Meanwhile, this methodology has been further developed so that absolute concentrations can be measured and thus quantitative images shown by AFM of mixtures homogeneously dispersed on the analyzed surface.

Acknowledgments

H.A. gratefully acknowledges JN-Circle colleagues for their continued encouragement of his research projects. This research was partially supported by the Conseil Régional des Pays de la Loire.

REFERENCES

1. Baughman RH, Zakhidov AA, Heer WA. *Science* 2002; **297**: 787.
2. Zhang M, Yudasaka M, Koshio A, Jabs C, Ichihashi T, Iijima S. *Appl. Phys. A* 2002; **74**: 7.
3. Gu Z, Peng H, Hauge RH, Smalley RE, Margrave JL. *Nano Lett.* 2002; **2**: 1009.
4. Jin Z, Sun X, Xu G, Goh SH, Ji W. *Chem. Phys. Lett.* 2000; **318**: 505.
5. Kumar S, Doshi H, Srinivasarao M, Park JO, Schiraldi DA. *Polymer* 2002; **43**: 1701.
6. Shaffer MSP, Windle AH. *Adv. Mater.* 1999; **11**: 937.
7. Iijima S. *Nature* 1991; **354**: 56.
8. Hiura H, Ebbesen TW, Tanigaki K, Takahashi H. *Chem. Phys. Lett.* 1993; **202**: 509.
9. Chandrabhas N, Sood AK, Sundarraraman D, Raju S, Raghunathan VS, Rao GVN, Sastry VS, Radhakrishnan TSR, Hariharan Y, Bharathi A, Sundar CS. *Pramana J. Phys.* 1994; **42**: 375.
10. Kastner J, Pichler T, Kuzmany H. *Chem. Phys. Lett.* 1994; **221**: 53.
11. Bacsa WS, Ugarte D, Chatelain A, Deheer WA. *Phys. Rev. B* 1994; **50**: 15 473.
12. Eklund PC, Holden JM, Jishi RA. *Carbon* 1995; **33**: 959.
13. Rao AM, Richter E, Bandow S, Chase B, Eklund PC, Williams KA, Fang S, Subbaswamy KR, Menon M, Thess A, Smalley RE, Dresselhaus G, Dresselhaus MS. *Science* 1997; **275**: 187.
14. Qian W, Liu T, Wei F, Yuan H. *Carbon* 2003; **41**: 1851.
15. Atalay H, Lefrant S. *J. Nanosci. Nanotechnol.* 2004; **4**: 744.
16. Long DA. *The Raman Effect*. Wiley: Chichester, 2002.
17. Dresselhaus MS, Dresselhaus G, Jorio A, Filho ASS, Saito R. *Carbon* 2002; **40**: 2043.
18. Zolyomi V, Kürti J, Grüneis A, Kuzmany H. *Phys. Rev. Lett.* 2003; **90**: 157 401.
19. Wang Y, Alsmeyer DC, McCreery RL. *Chem. Mater.* 1990; **2**: 557.
20. Maultzsch J, Reich S, Thomsen C. *Phys. Rev. B* 2001; **64**: 121 407.
21. Thomsen C, Reich S. *Phys. Rev. Lett.* 2000; **85**: 5214.
22. Brown SDM, Jorio A, Dresselhaus MS, Dresselhaus G. *Phys. Rev. B* 2001; **64**: 073 403.
23. Kataura H, Kumazawa Y, Maniwa Y, Ohtsuka Y, Sen R, Suzuki S, Achiba Y. *Carbon* 2000; **38**: 1691.
24. Holden JM, Zhou P, Bi XX, Eklund PC, Bandow S, Jishi RA, Chowdhury KD, Dresselhaus G, Dresselhaus MS. *Chem. Phys. Lett.* 1994; **220**: 186.
25. Pimenta MA, Marucci A, Empedocles S, Bawendi M, Hanlon EB, Rao AM, Eklund PC, Smalley RE, Dresselhaus G, Dresselhaus MS. *Phys. Rev. B* 1998; **58**: R16016.
26. Ferrari AC, Robertson J. *Phys. Rev. B* 2000; **61**: 14 095.
27. Lee YJ. *J. Nucl. Mater.* 2004; **325**: 174.
28. Tuinstra F, Koenig JL. *J. Chem. Phys.* 1970; **53**: 1126.
29. Gruber T, Zerda TW, Gerspacher M. *Carbon* 1994; **32**: 1377.
30. Battey DE, Slater JB, Wludyka R, Owen H, Pallister DM, Morris MD. *Appl. Spectrosc.* 1993; **47**: 1913.
31. Pellow-Jarman MV, Hendra PJ, Lehnert RJ. *Vib. Spectrosc.* 1996; **12**: 257.
32. Frost KJ, McCreery RL. *Appl. Spectrosc.* 1998; **52**: 1614.
33. Mann CK, Vickers TJ. *Appl. Spectrosc.* 1999; **53**: 856.
34. Fryling M, Frank CJ, McCreery RL. *Appl. Spectrosc.* 1993; **47**: 1965.
35. Strommen D, Nakamoto K. *Laboratory Raman Spectroscopy*. Wiley: New York, 1984.
36. Saito R, Takeya T, Kimura T, Dresselhaus MS, Dresselhaus G. *Phys. Rev. B* 1998; **57**: 4145.
37. Bandow S, Asaka S, Saito Y, Rao AM, Grigorian L, Richter E, Eklund PC. *Phys. Rev. Lett.* 1998; **80**: 3779.
38. Zhao X, Ando Y, Qin LC, Kataura H, Maniwa Y, Saito R. *Chem. Phys. Lett.* 2002; **361**: 169.
39. Pelletier MJ. *Appl. Spectrosc.* 2003; **57**: 20A.
40. Kubelka P, Munk F. *Z. Tech. Phys.* 1931; **12**: 593.
41. Nakamoto K. *Infrared and Raman Spectra of Inorganic and Coordination Compounds* (4th edn). Wiley: New York, 1986.
42. Tobin MC. *Laser Raman Spectroscopy*. Wiley: New York, 1971.
43. Tan P, Zhang SL, Yue KT, Huang F, Shi Z, Zhou X, Gu Z. *J. Raman Spectrosc.* 1997; **28**: 369.
44. Geng JF, Singh C, Shephard DS, Shaffer MSP, Johnson BFG, Windle AH. *Chem. Commun.* 2002; 2666.
45. Yan H, Li QW, Zhang J, Liu ZF. *Carbon* 2002; **40**: 2693.
46. Ito K, Kato T, Ona T. *J. Raman Spectrosc.* 2002; **33**: 466.
47. Atalay A, Lefrant S. In *Proceedings of the ICSM, Australia*. 2004; In press.
48. O'Connell MJ, Bachilo SM, Huffman CB, Moore VC, Strano MS, Haroz EH, Rialon KL, Boul PJ, Noon WH, Kittrell C, Ma J, Hauge RH, Weisman RB, Smalley RE. *Science* 2002; **297**: 593.